

Chemistry of Iron(III) in a Hemin-like Macrocyclic $[N_4]^{2-}$ Environment: Relationship between CT Absorption and EPR Spectra

Ernst-G. Jäger* and Heike Keutel

Institute of Inorganic and Analytical Chemistry, Friedrich-Schiller-University, Jena D-07743, Germany

Received March 5, 1997[⊗]

The visible/near-IR and EPR spectra of the octahedral low-spin diadducts of the ethylene-bridged complex 6,13-diethoxycarbonyl-5,14-dimethyl-1,4,8,11-tetraazacyclotetradeca-4,6,12,14-tetraenato[2⁻]iron(III) iodide (**1a-I**), the ethylene/phenylene **1b-I**, and the phenylene-bridged analogous complex **1c-I** were investigated as a function of the axial and equatorial ligands. **1a-I** forms octahedral low-spin diadducts in polar solvents (water, methanol) with a large variety of bases (pyridines, imidazoles, ammonia, amines, hydroxide, pseudohalides, sulfite, thiosulfate, nitrite, isonitriles, phosphines, phosphites, etc.). The diadducts show a characteristic sharp equatorial ligand (π) to ferric (t_{2g}) ion charge-transfer (CT) transition in the visible or near-IR. The energy of the maximum (E_{CT}) shows a bathochromic shift with increasing π acceptor strength and/or decreasing basicity of the axial ligands. The EPR spectra of the diadducts in frozen solution (77 K) are of rhombic type. In the case of the phosphorus ligand diadducts, a superhyperfine splitting was found, which indicates the coupling of two phosphorus nuclei with the unpaired electron of the iron(III). Using Taylor's model, the relative energies of the t_{2g} orbitals was calculated from the g values to characterize the symmetry of the ligand field. The low symmetry of the equatorial ligands is mainly responsible for tetragonal and rhombic ligand field distortion, which is in contrast to the more symmetric porphyrin ligands which effect only a tetragonal distortion. The splitting of the t_{2g} orbitals is greatly enlarged with increasing π acceptor ability of the axial ligand. In the order $[1a-X_2]^+$, $[1b-X_2]^+$, $[1c-X_2]^+$, $FeTPPX_2^+$, the energy E_{CT} and the t_{2g} orbital splitting decrease as the π conjugation of the equatorial ligand increases. In contrast to the investigations of hemoproteins, no positive correlation between E_{CT} and E_{EPR} (the energy of the Fe(III) hole relative to the baricenter of the t_{2g} 3d subshell) was found. Generally, the CT energy increases as the orbital splitting decreases.

Introduction

Iron porphyrins are important and widespread catalytic centers for biochemical reactions involved in the transport and metabolism of dioxygen (hemoglobin, myoglobin, cytochrome *c* oxidase, cytochrome P-450, peroxidases, catalases) as well as in charge-transferring (CT) processes (cytochromes *b*, *c*, *f*) and redox reactions (sulfite reductase, nitrite reductase, hydroxylamine oxidase, etc.).² Due to their biological significance, the porphyrins belong to the most intensively studied classes of coordination compounds. In recent years it has been shown that in the absence of a protein component some functions of heme enzymes can be modeled by iron porphyrins with special peripheral substituents.³ Compared to these extensive investigations, rather little is known about the more general effects of the macrocyclic $[N_4]^{2-}$ ligands in the equatorial plane on the properties of the iron central atom and especially on its axial reactivity. With the exception of iron phthalocyanines, which have a close structural relationship to the porphyrins, there are only few examples of iron complexes with non-porphyrin dianionic macrocyclic $[N_4]^{2-}$ ligands. Holm et al.,⁴ Riley and Busch,⁵ and Goedken and Park⁶ have all described iron(II)/(III) complexes of macrocyclic anionic Schiff base ligands **3–6**.

Nishida et al. published the EPR and Mössbauer spectra of low-spin iron(III) complexes of the types **7** with $[N_2O_2]^{2-}$ Schiff base ligands⁷ and **8** with dimethylglyoxime as the equatorial and imidazole as the axial ligands.⁸

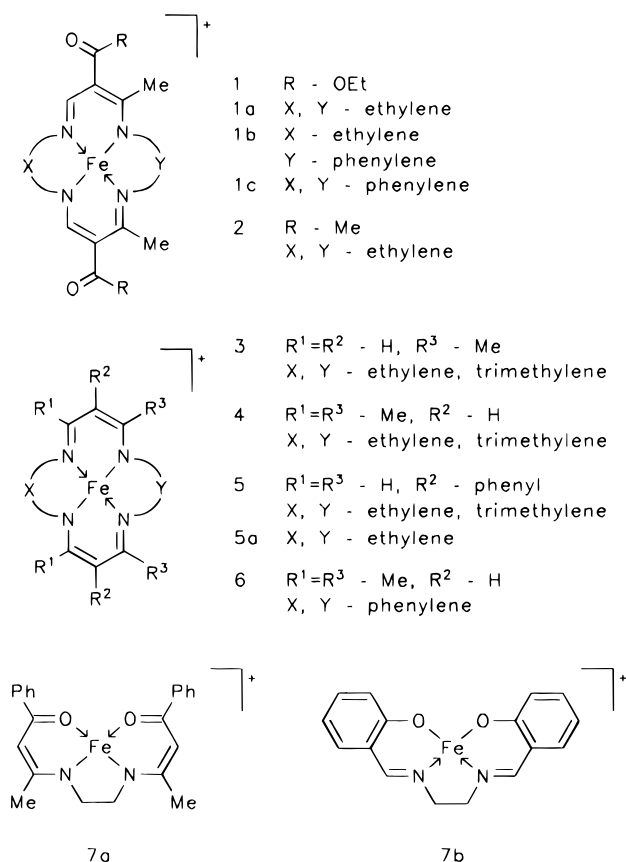
Some years ago we described the parent iron(II) complexes **1a** and **2**.^{9,10} Recently we reported on the corresponding iron(III) derivatives.^{10–12} The iodo derivatives of these iron(III) complexes (**1a-I**, **2-I**) are distinguished from **5** mainly by the free carbonyl groups in the meso position, which lead to some advantageous properties: (1) In contrast to the unsubstituted macrocycles **3** and **5**, the iron(III) derivatives are stable in air because the meso substituents protect the ligand from the electrophilic attack of dioxygen. (2) They are soluble without decomposition in water as well as in organic solvents. The ester derivative **1a** is more lipophilic, the acetyl derivative **2** more hydrophilic. While the iron(III) complexes **5** are water sensitive,⁴ **1a-I** and **2-I** are stable—even in strong alkaline aqueous solution. (3) Due to the reduced π system (compared to the porphyrin dianion), the ligand anions in **1a** and **2** are colorless. Therefore, the visible spectra of the complexes are dominated by a strong and sharp CT transition between the highest π orbital

[⊗] Abstract published in *Advance ACS Abstracts*, July 1, 1997.

(1) Friedrich-Schiller-University Jena.
 (2) Kostic, N. M. In *Electron Transfer Reactions in Metalloproteins*; Sigel, H., Sigel, A., Eds.; Marcel Dekker: New York, 1991; pp 129. *Degradation of Environmental Pollutants by Microorganisms and Their Metalloenzymes Metal Ions in Biological Systems*; Sigel, H., Ed.; Marcel Dekker: New York, 1992.
 (3) *Activation of Dioxygen and Homogeneous Catalytic Oxidation*; Barton, D. H. R., Martell, A. E., Sawyer, D. T., Eds.; Plenum Press: New York, 1993.
 (4) Koch, S.; Holm, R. H.; Frankel, R. B. *J. Am. Chem. Soc.* **1975**, *97*, 6714–6722.

(5) Riley, D. P.; Busch, D. H. *Inorg. Chem.* **1984**, *23*, 3235–3241.
 (6) Goedken, V. L.; Park, J. J. *Chem. Soc., Chem. Commun.* **1975**, 214–215.
 (7) Nishida, Y.; Oshio, S.; Kida, S. *Inorg. Chim. Acta* **1977**, *23*, 59–61.
 (8) Nishida, Y.; Oshio, S.; Kida, S.; Maeda, Y. *Inorg. Chim. Acta* **1978**, *26*, 207–211.
 (9) Jäger, E.-G.; Stein, E.; Gräfe, F.; Schade, W. *Z. Anorg. Allg. Chem.* **1985**, *526*, 15–28.
 (10) Jäger, E.-G.; Keutel, H.; Rudolph, M.; Krebs, M.; Wiesemann, F. *Chem. Ber.* **1995**, *128*, 503–514.
 (11) Jäger, E.-G.; Gräfe, F. *Z. Anorg. Allg. Chem.* **1988**, *561*, 25–37.
 (12) Jäger, E.-G.; Hähnel, H.; Klein, H.-F.; Schmidt, A. *J. Prakt. Chem.* **1991**, *333*, 423–430.

Chart 1



of the equatorial ligand and the t_{2g} orbitals of the iron(III)¹² so that the reactions on the central atom can be readily investigated using spectrophotometric methods^{13,14} (e.g., equilibrium reactions of stepwise axial ligand substitution). (4) Unlike **5**, the electron-withdrawing effect of the meso carbonyl substituents results in a stabilization of the lower oxidation state and a strongly increased Lewis acidity of the axial coordination sites (i.e., the ability to bind axial ligands). Consequently, it was possible to obtain adducts with a broader variety of axial ligands, including ligands with reducing properties (CN^- , $\text{S}_2\text{O}_3^{2-}$, SO_3^{2-} , NO_2^- , PR_3 , $\text{P}(\text{OR})_3$, isonitriles, acetylides, etc.).¹² (5) In addition to the miscellaneous octahedral derivatives, numerous pentacoordinated intermediate-spin ($S = 3/2$) or high-spin species are formed with halides, pseudohalides, carboxylates, and μ -oxide.¹² Heterogeneous equilibria between octahedral anionic diadducts $[\text{Fe-X}_2]^-$ in water and pentacoordinated neutral species Fe-X in chloroform or benzene exist in some cases (e.g., with F^- , SCN^- , and N_3^-).

As mentioned above, the optical spectra in the case of the complex **1a** yield valuable information about the electronic effects of axial ligands.¹² Therefore, in this paper our interest is focused on the influence of a broad series of axial ligands on the electronic properties of iron(III) in an equatorial $[\text{N}_4]^{2-}$ environment.

EPR spectroscopy provides another widely used technique to describe the symmetry and the orbital splitting of low-spin iron(III) complexes. The spectra are generally characterized by three g values. Depending on the particular orientation of the axial ligands to each other and to the porphyrin ligand, three

Table 1. g Values of Some Hemin Enzymes and Relevant Models

	axial ligand	g_1	g_2	g_3	solvent	ref
cyt <i>b</i> ₅ native	his	1.43	2.23	3.03		43
cyt <i>b</i> ₅₆₆	his	3.75–				16
			3.78			
sulfitoreductase	his/S	1.77	2.36	2.44		21
protohämiline	Him	1.51	2.24	3.02		16
FeTPP ⁺	Meim	1.549	2.294	2.886	CHCl_3	43
FeTPP ⁺	dmap	1.657	2.284	2.786	CH_2Cl_2	43
FeTPP ⁺	5Cl-Meim	1.533	2.308	2.884	CH_2Cl_2	43
FeTPP ⁺	PMe ₃	1.680	2.088	2.687	crystalline	44
FeTPP ⁺	2Meim	1.188	1.74	3.399	CH_2Cl_2	43
FeTPP ⁺	py	1.2	1.7	3.4	CH_2Cl_2	43
FeTMP ⁺	Meim	1.571	2.325	2.886	CH_2Cl_2	21
FeTMP ⁺	4CNpy		1.56	2.53	crystalline	21
5a	Meim	1.99	2.04	2.10	$\text{DMF}/\text{CH}_2\text{Cl}_2$	4
7a	Him	1.94	2.10	2.40	crystalline	7
7b	Him	1.98	2.21	2.44	crystalline	7
$\text{Fe}(\text{dgm})_2^+$	Him		1.96	2.28	DMSO	8

types of spectra were found in porphyrins and hemoproteins:¹⁵ (1) The “normal” rhombic spectra show g values in the range of 3, 2.3, and 1.5. In this case the axial ligand planes are parallelly aligned.^{16–18} (2) The “strong g_{max} ” spectra exhibit one g value >3.3 .^{19,20} Here the orientation of the axial ligands are perpendicular to each other. In (1) and (2) the d-electron configuration is $(d_{xy})^2 (d_{xz}, d_{yz})^3$. (3) “Hindered” porphyrins (e.g., tetramesitylporphyrin) with very weak axial ligands (4CNpy) show axial spectra ($g = 2.53, 1.56$). In this case, the iron center shows a $(d_{xz}, d_{yz})^4 (d_{xy})^1$ configuration.^{21,22} This d-electron configuration was also found in complexes with donor ligands stronger than porphyrins, such as Schiff bases^{4,7} (**5**, **7**) and dimethylglyoxime⁸ (**8**). The spectra exhibit g values of ~ 2 . The g values of some hemoproteins and relevant models are listed in Table 1.

Using Taylor’s “ t_{2g} hole model”, the relative energies of the t_{2g} orbitals can be calculated from the g values in units of the spin-orbit coupling constant λ , which is directly related to the tetragonal (Δ) and rhombic (V) splitting.²³

In order to predict the axial coordination of hemoproteins, Peisach and Blumberg²⁴ developed a plot of V/Δ vs V/λ . The data points of enzymes with the same axial coordination are localized in the same clusters of the diagram. Schejter and Eaton²⁵ and Gadsby and Thomson²⁶ have tried to correlate the energy of the $\pi(\text{eq ligand})$ to $(t_{2g})^5$ transition (E_{CT}) with the splitting parameters calculated from the EPR data. However, in the case of porphyrins, the CT band is located in the near-

(15) Scheidt, W. R.; Lee, J. Y. *Struct. Bonding* **1987**, *64*, 1–70.(16) Walker, F. A.; Huynh, B. H.; Scheidt, W. R.; Osvath, S. R. *J. Am. Chem. Soc.* **1986**, *108*, 5288–5297.(17) Quinn, R.; Valentine, J. S.; Bryn, M. P.; Strouse, C. E. *J. Am. Chem. Soc.* **1987**, *109*, 3301–3308.(18) Soltis, S. M.; Strouse, C. E. *J. Am. Chem. Soc.* **1988**, *110*, 2824–2829.(19) Safo, M. K.; Gupta, G. P.; Walker, F. A.; Scheidt, W. R. *J. Am. Chem. Soc.* **1991**, *113*, 5497–5510.(20) Hatano, K.; Safo, M. K.; Walker, F. A.; Scheidt, W. R. *Inorg. Chem.* **1991**, *30*, 1643–1650.(21) Safo, M. K.; Gupta, G. P.; Watson, C. T.; Simonis, U.; Walker, F. A.; Scheidt, W. R. *J. Am. Chem. Soc.* **1992**, *114*, 7066–7075.(22) Safo, M. K.; Walker, F. A.; Raitsimring, A. M.; Walters, W. P.; Dolota, D. P.; Debrunner, P. G.; Scheidt, W. R. *J. Am. Chem. Soc.* **1994**, *116*, 7760–7770.(23) Taylor, C. P. S. *Biochim. Biophys. Acta* **1977**, *491*, 137–149.(24) Blumberg, W. E.; Peisach, J. In *Structure and Function of Macromolecules and Membranes*; Chance, B., Yonetani, T., Mildvan, A. S., Eds.; Academic Press: New York, 1971; Vol. II, p 215.(25) Schejter, A.; Eaton, W. A. *Biochemistry* **1984**, *23*, 1081–1084.(26) Gadsby, P. M. A.; Thomson, A. J. *J. Am. Chem. Soc.* **1991**, *112*, 5003–5011.(27) Jäger, E.-G. *Z. Chem.* **1968**, *8*, 30–31, 470–471.(13) Jäger, E.-G.; Schweder, B.; Radzuweit, S. *Z. Chem.* **1988**, *28*, 152–153.(14) Jäger, E.-G.; Liehr, J.; Morich, E.; Dix, A. *Proceedings of the 12th Conference on Coordination Chemistry*, 6–9 June 1989, pp 123–128.

infrared region (700–3000 nm) and, due to the splitting of the highest ligand π orbitals, shows some shoulders. Thus, in some cases it is difficult to make a clear assignment of the CT energy. Schejter and Thomson used materials (e.g., myoglobin derivatives) with one histidine and one other axial ligand.

With complex **1a**, we obtained more general information about a possible correlation based on the well-defined energies of the sharp visible CT band. The complexes **1a**, **1b**, and **1c** were used to investigate the influence of a changed π system on the visible absorption and the EPR spectra.

Experimental Section

Chemicals. The solvents for synthesis of the complexes and for measurements were distilled under an argon atmosphere prior to use. Methanol was dried by reaction with activated magnesium and THF²⁸ by distillation from sodium benzophenone ketyl. The bases used as axial ligands were obtained from Merck and Aldrich, respectively. 4-(Dimethylamino)pyridine (dmap), 3-cyanopyridine (3CNpy), nicotinamide (na), nicotinic acid methyl ester (name), pyrazine (pyz), imidazole (Him), 2-methylimidazole (2Meim), cyclohexylisocyanide (cNC), toluene-4-sulfonylmethylisocyanide (tNC), NaN₃, KSCN, KCN, and KOH were used without further purification. Acetonitrile, aniline, and *N*-methylimidazole (Meim) were distilled. Pyridine was distilled from KOH. Ammonia and methylamine (MeNH₂) were used as solution in dried methanol. Trimethylphosphine (PMe₃) was synthesized by published methods.²⁹ Tributylphosphine (PBu₃) and Triethyl phosphite (P(OEt)₃) were distilled under argon. All solutions used for measurements with phosphines were handled under argon.

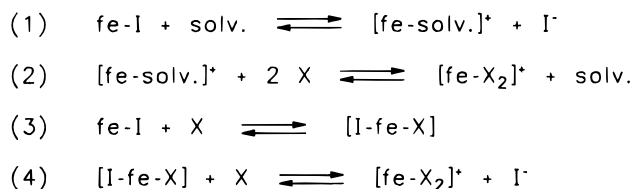
Physical Measurements and Procedures. Ultraviolet, visible, and near-infrared spectra were measured with a Varian Cary 5 spectrophotometer at 293 K. In the case of the spectra at 183 K, a Specac variable-temperature cell P/N was used. EPR spectra were obtained in frozen solutions at 77 or 150 K, respectively, with a ZWG ERS 300 spectrometer in the X band at 9.35 GHz, equipped with a flowing nitrogen variable-temperature controller. The *g* values are quoted relative to an external standard (DPPH; *g* = 2.0036).

The spectrophotometric and EPR measurements of diadducts were carried out in methanol or water. In the case of PMe₃, THF was used as an additional solvent. The concentrations of the complexes were about (1–1.5) × 10⁻⁴ (**1a**) and 7 × 10⁻⁴ M (**1b,c**) for UV–visible and (2–5) × 10⁻³ M for EPR measurements. The axial ligands were used in such a concentration that a quantitative (>99%) formation of diadducts could be expected. These concentrations were determined by spectrophotometric titrations for the step-by-step addition of axial ligands at room temperature. The exchange of solvent and iodide by an appropriate base to form the diadducts is in general exergonic and also exothermic. Thus, the quantitative formation of the adducts could also be assumed for the low temperatures of EPR measurements.

Synthesis. The macrocyclic ligand of **1a**,²⁷ the Fe(III) complex **1b-I**,¹⁰ and the Fe(II) complex **1c**³⁰ were prepared as previously described.

1a-I:¹² Iron(II) acetate³¹ (1.74 g, 0.01 mol) and free ligand (3.64 g, 0.01 mol) were boiled in 50 mL of methanol. The reaction mixture was red (iron(II) complex). Iodine (1.27 g, 0.005 mol) and NaI (1.2 g, 0.008 mol) in 30 mL of methanol were added. The solution was boiled for 15 min. The product was crystallized by cooling the mixture. After collection and washing with a small volume of cool methanol, black-violet needles were obtained (**1a-I**: 4.6 g, 85%).

Scheme 1



1c-I. **1c** (2 g, 0.004 mol) was dissolved in 50 mL of DMF. Iodine (0.5 g, 0.004 mol) and NaI (1 g, 0.007 mol) in 20 mL of DMF were added. The solution was stirred 1 h at 370 K. The reaction mixture was cooled and the black crystals were collected and washed with methanol (**1c-I**: 1.75 g, 70%). An extraction with toluene for further purification was done. Anal. Calcd for C₂₆H₂₆N₄FeO₄: C, 48.69; H, 4.09; N, 8.74; Fe, 8.71; I, 19.79. Found: C, 48.66; H, 4.01; N, 8.83; Fe, 8.82; I, 20.03.

Although the isolated pure iodides of the complexes are stable on air, the synthetic procedures must be carried out under anaerobic conditions to ensure that the undissociated iodide can be formed before the formation of the acetates or the μ -oxo derivatives from the iron(III) complexes occur because they are more air sensitive.

[1a-py₂]ClO₄ and [1a-meim₂]ClO₄. **1a-I** (0.11 g, 0.2 mmol) and NaClO₄ (0.5 g, 4 mmol) were dissolved in 3 mL of pure base (py, meim). The addition of 10 mL of H₂O led to the crystallization of the product. After collection and washing with a small amount of H₂O, green microcrystalline solids were obtained (74 mg, 55%; 93 mg, 68%). Anal. Calcd for C₂₈H₃₆N₆ClFeO₈: C, 49.75; H, 5.37; N, 12.44; Fe, 8.26. Found: C, 49.87; H, 5.36; N, 12.24; Fe, 8.14. Anal. Calcd for C₂₆H₃₈N₈ClFeO₈: C, 45.79; H, 5.62; N, 16.44; Fe, 7.53. Found: C, 45.60; H, 5.53; N, 16.22; Fe, 7.65.

[1a-Him₂]PF₆ was prepared as previously described.³²

Results

Magnetic Behavior. The iodides **1-I** are intermediate-spin complexes with magnetic moments of 3.56 (**1a-I**),¹² 4.06 (**1b-I**),¹⁰ and 4.01 μ_B (**1c-I**) at 295 K without any temperature dependence of the magnetic moment down to 77 K.^{33,34} This is in agreement with a ⁴A₂ (*S* = 3/2) ground state stabilized by the strong tetragonal distortion effected by the pentacoordination with the halide as a relatively weak axial ligand.³⁵ The same behavior was found in the case of the iodides of the parent complexes **5** and **3** without the free carbonyl substituents.^{4,5} In contrast to this, the halides of iron(III) porphyrins show high-spin character.

In the case of porphyrin complexes and for **1** and **5**, the stronger axial ligands, such as imidazoles and pyridines, lead to octahedral low-spin complexes. The magnetic moments of the isolated diadducts are ~1.8 μ_B (**[1a-py₂]ClO₄**), 1.83 μ_B ; **[1a-Meim₂]ClO₄**, 1.87 μ_B ; **[1a-Him₂]PF₆**, 1.78 μ_B).

Spectrophotometry. In polar solvents (e.g., water, methanol, or THF) the complex **1a**⁺ forms octahedral diadducts with a large variety of bases. The formation of the diadducts follows the Scheme 1.

The iodide dissociates in polar solvents,³⁶ and the solvent molecules are added (reaction 1). While the majority of diadducts are formed as shown in reaction 2, the formation of phosphine and phosphite diadducts follows reaction 3 and 4. In the case of **[1a-(P(OEt)₃)₂]⁺** the visible absorption band of **[I-1a-(P(OEt)₃)₂]⁺** is at 746 nm (**[1a-solv.]⁺**, 521 nm; **[1a-(P(OEt)₃)₂]⁺**,

(28) Abbreviations: TPP, meso-tetraphenylporphyrin; TMP, meso-tetramesitylporphyrin; dgm, diglyoximate; X, unspecified axial ligand; R, unspecified organic substituent; DMF, *N,N*-dimethylformamide; THF, tetrahydrofuran; MeOH, methanol; py, pyridine; dmap, 4-(dimethylamino)pyridine; 3CNpy, 3-cyanopyridine; na, nicotinamide; name, nicotinic acid methyl ester; pyz, pyrazine; Him, imidazole; Meim, *N*-methylimidazole; 2Meim, 2-methylimidazole; MeNH₂, methylamine; cNC, cyclohexylisocyanide; tNC, toluene-4-sulfonylmethylisocyanide; PMe₃, trimethylphosphine; PBu₃, tributylphosphine; P(OEt)₃, triethyl phosphite.

(29) We thank H.-F. Klein for providing the PMe₃.

(30) Müller, K.; Jäger, E.-G. *Z. Anorg. Allg. Chem.* **1989**, *577*, 195–205.

(31) Heyn, B.; Hipler, B.; Kreisel, G.; Schreer, H.; Walther, D. *Anorganische Synthesechemie*; Springer Verlag: Heidelberg, 1986; p 142.

(32) Wiesemann, F.; Wonnemann, R.; Krebs, B.; Keutel, H.; Jäger, E.-G. *Angew. Chem., Int. Ed. Engl.* **1994**, *33*, 1363–1366.

(33) Gülich, M., personal communications.

(34) Keutel, H. Thesis, Friedrich-Schiller-University Jena, 1994.

(35) Reed, C. A.; Mashiko, T.; Bentley, S. P.; Kastner, M. E.; Scheidt, R. W.; Spartialian, K.; Lang, G. *J. Am. Chem. Soc.* **1979**, *101*, 2948–2958.

(36) The dissociation in water is detectable by measurements of conductivity.

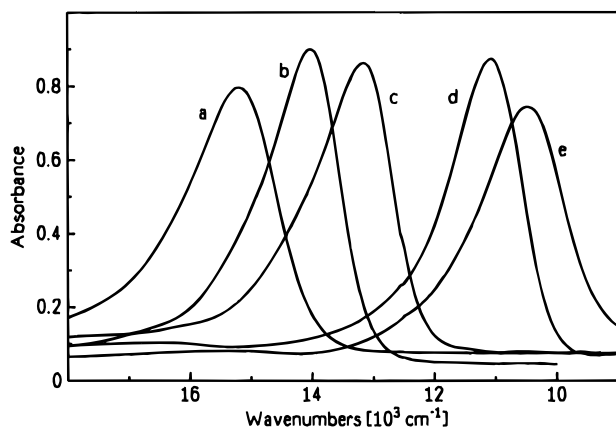


Figure 1. Visible spectra of [1a-X₂]⁺ (*c* ~ 10⁻⁴ mol L⁻¹) in methanolic solutions. X = (a) NH₃, (b) Him, (c) py, (d) P(OEt)₃, and (e) tNC.

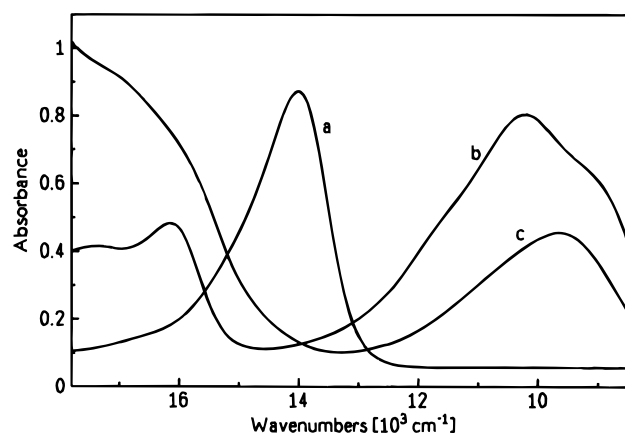


Figure 2. Visible/near-IR spectra of (a) [1a-Meim₂]⁺ (*c* ~ 10⁻⁴ mol L⁻¹), (b) [1b-Meim₂]⁺ (*c* ~ 7 × 10⁻⁴ mol L⁻¹), and (c) [1c-Meim₂]⁺ (*c* ~ 7 × 10⁻⁴ mol L⁻¹) in methanolic solutions.

887 nm). By adding other ligands, only the bands of [1a-solv]⁺ and [1a-X₂]⁺ are found. Bands of possible intermediate species, like [1a-solv,X]⁺ or [I-1a-X], are not observed.

In the cases of py, meim, and Him, the diadducts could be isolated as solids. The visible spectra in solution are nearly identically with those of the substances in remission.

The complexes 1b-I and 1c-I form octahedral low-spin diadducts with an excess of Meim as well.

The spectra of the complexes [1a-X₂]⁺ are dominated by a strong absorption (ϵ , (5–15) × 10³ L cm⁻¹ mol⁻¹). The location of the relatively sharp band is very much dependent on the axial ligand and extends from the ultraviolet up to the near-infrared border of the visible spectral range. The colors of the complex solutions vary correspondingly from pale yellow, orange, red, violet, blue, turquoise, and green on up to pale gray. With the strong donors OH⁻ or MeO⁻ as axial ligands, the band occurs at short wavelengths while ligands known as π acceptors (py < CNpy < P(OEt)₃ < tNC) induce an increasing bathochromic shift. In the case of the complexes [1b-Meim₂]⁺ and [1c-Meim₂]⁺, the analogous absorption is bathochromically shifted to the near-infrared and split. The extinction coefficients are 10³ and 5 × 10² L cm⁻¹ mol⁻¹. Figures 1 and 2 show the spectra of some diadducts. The absorption maxima are collected in Table 2. The analogous values for the acetyl-substituted complex 2 (measured in water) are listed in Table 3.

The MeO⁻ diadduct of 1a shows a thermochromic behavior (see Figure 3), probably resulting from a spin change similar to that described for the Schiff base complexes of the salen

Table 2. Spectroscopic Data of [1a-X₂]⁺, [1b-Meim₂]⁺, and [1c-Meim₂]⁺

X	pK _a (HX) ^a	c _{base} , ^b mol/L	λ_{\max} , nm	g values (A, G) ^c		
				g ₁	g ₂	g ₃
MeO ⁻		0.5	589 ^d	1.969	2.140	2.175
N ₃ ⁻	4.92	<i>e</i>	648	1.977	2.139	2.174
SCN ⁻	0.85	<i>e</i>	718	1.973	2.125	2.162
CN ⁻	9.21	0.01	767	1.982	2.077	2.178
NH ₃	9.25	0.5	657	1.979	2.111	2.169
MeNH ₂		0.5	659	1.978	2.091	2.163
Him	6.65	0.5	713	1.978	2.092	2.164
				1.984 ^f	2.086	2.152
Meim	7.33	0.5	714	1.983	2.088	2.160
2Meim	7.56	1	706	1.982	2.090	2.160
py	5.10	1	760	1.988	2.064	2.140
dmap		0.5	724	1.979	2.089	2.156
na		1.5	770	1.987	2.064	2.140
name	3.13	1.5	779	1.987	2.061	2.133
3CNpy	1.14	1.5	786	1.988	2.057	2.134
pyz	0.65	<i>e</i>	794	1.993	2.054	2.126
PMe ₃	8.65	1.5	862	1.990	2.040	2.154
				(22)	(24)	(18.5)
PBu ₃	8.43	1.5	840	1.993	2.041	2.148
				(22)	(23)	(21)
P(OEt) ₃	3.31	1.5	887	1.998	2.029	2.133
				(34)	(31.5)	(28.5)
cNC		1.5	905	1.994	2.050	2.121
tNC		<i>e</i>	956	1.993	2.044	2.111
[1b-Meim ₂] ⁺		0.5	979 ^g	1.960	2.134	2.212
[1c-Meim ₂] ⁺		0.5	1038 ^h	1.899	2.136	2.424

^a Sillen, L. G. *Stability Constants of Metal-Ion Complexes with Solubility Products of Inorganic Substances Part 1: Organic Ligands*; The Chemical Society: Burlington House: London, 1957. Schoefield, K. *Hetero-Aromatic Nitrogen Compounds*; Plenum Press: New York, 1967; p. 146. *Handbook of Chemistry and Physics*, 73rd ed.; CRC Press: Boca Raton, FL, 1992; Landolt-Börnstein II/7; p. 839. Rahman, M. M.; Lin, H. Y.; Prock, A.; Giering, W. P. *Organometallics* **1987**, 6, 650–658. ^b In methanol. ^c Superhyperfine coupling constants with ³¹P. ^d 183 K. ^e Saturated solutions. ^f Crystalline [1a-Him₂]PF₆ ^g sh, 853, 1115 nm. ^h sh, 907 nm.

Table 3. Spectroscopic Data of [2-X₂]⁺

X	c _{base} , ^a mol/L	λ_{\max} , nm	g values		
			g ₁	g ₂	g ₃
MeO ⁻	0.5 ^b	424	1.962	2.149	2.213
OH ⁻	0.5	513	1.965	2.149	2.196
CN ⁻	0.01	772	1.977	2.074	2.160
NO ₂ ⁻	1	781	1.989	2.056	2.162
NH ₃	0.5	651	1.971	2.136	2.194
aniline	1	694	1.981	2.102	2.176
Him	0.5	704	1.970	2.107	2.180
im ⁻	0.5	660	1.956	2.152	2.198
Meim	0.5	699	1.972	2.108	2.183
py	1	752	1.980	2.074	2.160
albumin	2.5 ^c	709	1.969	2.118	2.186
globulin	1.25 ^c	709	1.969	2.115	2.187

^a In water. ^b In methanol. ^c In percent.

type.³⁷ The blue low-temperature form is a low-spin complex as well (see EPR data), while the yellow room-temperature form is presumably a high-spin complex.

EPR Measurements. The diadducts [1a-X₂]⁺, [2-X₂]⁺, [1b-Meim₂]⁺, and [1c-Meim₂]⁺ give the typical rhombic EPR spectra of octahedral low-spin iron(III) complexes with tetradentate equatorial chelate ligands. Figure 4 shows the spectra of [1a-Meim₂]⁺ and [1a-(P(OEt)₃)₂]⁺. In the case of phosphorus ligands, a superhyperfine coupling (between the electron spin of iron(III) and the nuclear spin of ³¹P (*I* = 1/2)) was observed.

(37) Kennedy, B. J.; McGrath, A. C.; Murray, K. S.; Skelton, B. W.; Whrite, A. H. *Inorg. Chem.* **1987**, 26, 483–495.

Table 4. Charge-Transfer Energies of $[\mathbf{1a-X}_2]^+$ and Relative Energies of the t_{2g} Orbitals of $[\mathbf{1a-X}_2]^+$, Some Hemin Enzymes and Other Models (Definition of E : Scheme 3; $E_0 = 0$)

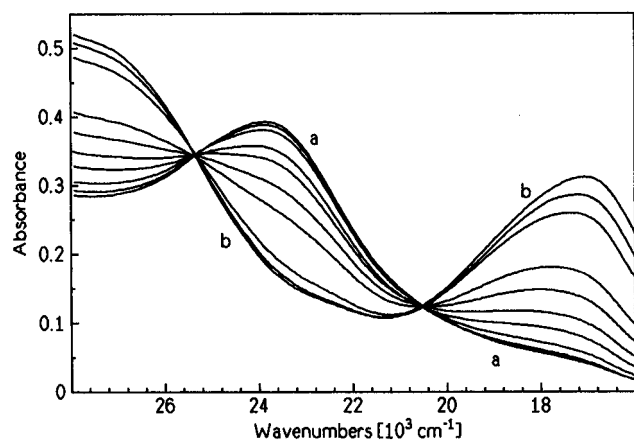
X	E_{CT} , 10^3 cm^{-1}	E_1 , 10^3 cm^{-1}	E_2 , 10^3 cm^{-1}	E_{EPR} , 10^3 cm^{-1}	$a^2 + b^2 + c^2$ a
MeO ⁻	16.98 ^b	4.3 ± 0.1 ^c	5.3 ± 0.2	3.2 ± 0.1	0.996
N ₃ ⁻	15.43	4.5	5.6	3.4	0.999
SCN ⁻	13.93	4.7	5.9	3.5	0.996
CN ⁻	13.04	4.4 ± 0.1	9.4 ± 0.6	4.6 ± 0.2	0.998
NH ₃	15.22	4.6	6.8	3.8	0.998
MeNH ₂	15.17	4.7	7.8	4.2	0.997
Him	14.03	4.7	7.8	4.2	0.996
Him ^d		5.2	8.7	4.6	0.998
Meim	14.05	4.9 ± 0.2	8.4 ± 0.5	4.4 ± 0.2	0.998
2Meim	14.16	4.9	8.2	4.4	0.998
py	13.14	5.6 ± 0.2	11.5 ± 0.5	5.7 ± 0.4	0.998
dmap	13.81	4.9	8.0	4.3	0.996
na	12.99	5.6	11.3	5.6	0.998
name	12.84	5.8	11.7	5.8	0.998
CNpy	12.72	5.8	12.6	6.1	0.998
pyz	12.59	6.4	14.1	6.8	1.000
PMe ₃	11.60	5.2	17.0	7.5	0.999
PBu ₃	11.90	5.5	18.0	7.8	1.000
P(OEt) ₃	11.27	6.2 ± 0.3	28.0 ± 5.0	11.0 ± 2.0	1.002
cNC	11.05	6.6	15.3	7.3	1.000
tNC	10.46	7.1	16.7	8.0	0.999
$[\mathbf{1b-Meim}_2]^+$	10.21	3.6 ± 0.1 ^f	5.3 ± 0.3	2.9 ± 0.1	0.994
$[\mathbf{1c-Meim}_2]^+$	9.63	1.8 ± 0.1 ^g	4.3 ± 0.3	2.0 ± 0.1	0.992
$[\mathbf{5a-Meim}_2]^+$		7.6	17.0		
$[\mathbf{7a-Meim}_2]^+$		2.0	6.2		
FeTPP(Meim) ₂ ⁺	8.52/6.58 ^h	0.8	1.7		
FeTPP(dmap) ₂ ⁺		0.9	1.9		
FeTPP(5Cl-Meim) ₂ ⁺		0.8	1.6		
FeTPP(PMe ₃) ₂ ⁺		1.4	2.8		
cyt <i>b</i> ₅ ^e		0.7	1.6		
sulfite reductase		1.6	1.8		

^a Normalization condition. ^b 183 K. ^c Error in the case $\Delta g = \pm 0.003$.

^d Crystalline $[\mathbf{1-Him}_2]\text{PF}_6$. ^e Calculated from literature data (Table 1).

^f Error in the case $\Delta g = \pm 0.005$. ^g Error in the case $\Delta g = \pm 0.01$.

^h Reference 46.

**Figure 3.** Visible/near-IR spectra of $[\mathbf{1a-(MeO)}_2]^-$ and dependence on the temperature: (a) 303 K; (b) 200 K.

The coupling constant increases as the π acceptor strength of the axial P ligand (PMe₃, PBu₃ < P(OEt)₃) increases. The g values and the coupling constants (A) are listed in Table 2.

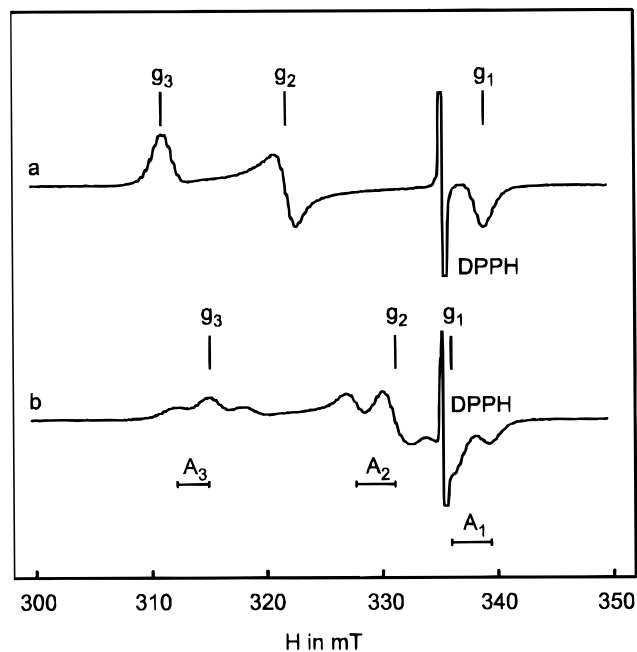
The g values may be used to calculate the relative energies of the t_{2g} orbitals (d_{xy} , d_{xz} , d_{yz}) as outlined by Griffith,³⁸ Kotani,³⁹ Weissbluth,⁴⁰ Bohan,⁴¹ and Taylor.²³ In this paper, Taylor's treatment was used.

(38) Griffith, J. S. *The Theory of Transition Metal Ions*; Cambridge University Press: New York, 1961; p 363.

(39) Kotani, M. *Rev. Mod. Phys.* **1963**, *35*, 717–723.

(40) Weissbluth, M. *Struct. Bonding (Berlin)* **1967**, *2*, 1–125.

(41) Bohan, T. L. *J. Magn. Reson.* **1977**, *26*, 109–118.

**Figure 4.** EPR spectra of (a) $[\mathbf{1a-Meim}_2]^+$ and (b) $[\mathbf{1a-(P(OEt)}_3)_2]^+$ ($c \sim 5 \times 10^{-3} \text{ mol L}^{-1}$) as methanolic glasses.

The underlying model requires that covalent bonding is negligible. However, it is well-known that covalent bonding plays an important role for porphyrin and Schiff base complexes. So π bonding is discussed to describe the effect of the orientation of the axial ligands in low-spin iron(III) porphyrins. Nevertheless, the model showed good results for the calculation of the splitting parameters of t_{2g} orbitals.^{16–22} Therefore, this theory was used to analyze the EPR spectra of $[\mathbf{1a-X}_2]^+$, $[\mathbf{1b-Meim}_2]^+$, and $[\mathbf{1c-Meim}_2]^+$ as well. On this basis, a comparison of porphyrins and Schiff base complexes was also possible.

The analysis of the g values was made in terms of a distorted octahedral, low-spin (t_{2g})⁵ complex. The effect of spin-orbit coupling and the distorted octahedral symmetry results in three Kramer's doublets. The ground state of this configuration is one doublet arising from a positive hole occupying the t_{2g} orbitals. The two corresponding wave functions (for α and β spin) are linear combinations of the three states with coefficients a (d_{yz}), b (d_{xz}), and c (d_{xy}). It can then be shown that

$$a = \frac{g_z + g_y}{4K}, \quad b = \frac{g_z - g_x}{4K}, \quad c = \frac{g_y - g_x}{4K} \quad (1)$$

where

$$4K = \sqrt{8(g_x + g_y + g_z)}$$

From these quantities, the relative energies of t_{2g} orbitals can be determined.

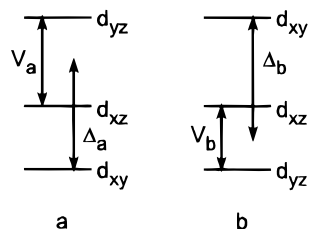
$$\frac{E_0}{\lambda} = 0, \quad \frac{E_1}{\lambda} = \frac{g_x}{g_z + g_y} + \frac{g_y}{g_z - g_x}, \quad \frac{E_2}{\lambda} = \frac{g_x}{g_z + g_y} + \frac{g_z}{g_y - g_x} \quad (2)$$

The distortion parameters are

$$\frac{V}{\lambda} = E_1, \quad \frac{\Delta}{\lambda} = E_2 - \frac{E_1}{2} \quad (3)$$

However, it is neither possible to assign the measured g values to g_x , g_y , and g_z , nor to define their sign from the powder spectra. By the substitution of all 48 combinations of three g values

Scheme 2



into (1), only six combinations satisfy the conditions²³

$$g_z + g_y > g_x, \quad a^2 + b^2 + c^2 = 1 \quad (4)$$

Only two at any one time are different in the sign of V/λ . This corresponds to a change of the d_{xz} and d_{yz} orbitals. In this case, the combinations with $V/\lambda > 0$ were chosen. The case $V > 2\Delta$ was excluded, too. The two possible combinations (a) $g_x = g_1, g_y = g_2, g_z = g_3$; (b) $g_x = -g_3, g_y = g_2, g_z = -g_1$ correspond to the energy level diagram represented in Scheme 2.

Case a refers to the electron configuration $(d_{xy})^2 (d_{xz}d_{yz})^3$ and case b to $(d_{xz}d_{yz})^4 (d_{xy})^1$. In both cases, the energy differences are the same. Using only the powder spectra, a definite assignment is not possible. The wide variety of axial ligands (strong donors \rightarrow strong π acceptors) can cause a change of the electron configuration within the investigated ligand adducts. Therefore, the discussion is restricted to the relative energies E_1 and E_2 . The values⁴² are listed in Table 3.

Discussion

The following discussion concerns the influence (1) of different axial ligands and (2) of the change of the bridges X, Y (and the thereby produced extension of the π system in the equatorial ligand) on the CT absorption band and its relation to the EPR spectra. Complex **2**, which differs from **1** only in the peripheric carbonyl group R², shows nearly identical properties to **1a**. Its spectroscopic data are not discussed in detail. Gradual differences can be seen from the tables.

Spectrophotometry. The strong absorption band of the adducts $[\mathbf{1a-X}_2]^+$ in the visible/near-IR region can only be interpreted as a charge-transfer absorption. The extinction coefficients exclude an assignment to d-d transitions, and the equatorial ligand dianion does not show any absorption in this region. The dependence on the axial ligands does not hint at an axial ligand to metal transition (no correlation with ionization potentials, base strengths, etc.). In agreement with the assignment of the near-infrared band of low-spin iron(III) porphyrins and hemoproteins to an equatorial ligand (π) to ferric (t_{2g})⁵ ion charge transfer, we assume an analogous transition for complexes $[\mathbf{1a-X}_2]^+$. The lower extension of the π system of the equatorial ligand dianion in **1a** explains the existence of only one CT band and the stabilization of the π HOMO in comparison to the porphyrin anion. Additionally, the Schiff base macrocycles are stronger σ and π donors and weaker π acceptors than the porphyrins. This effects an increase in the energy of the central atom orbitals. Both effects explain the higher charge-transfer energy E_{CT} (Table 4) and the hypsochromic shift of the CT band.

A comparison of the complexes **1a**, **1b**, **1c**, and FeTPP reveals that the increasing π conjugation of the equatorial ligand in the order $[\mathbf{1a-Meim}_2]^+ < [\mathbf{1b-Meim}_2]^+ < [\mathbf{1c-Meim}_2]^+ < [\text{FeTPP-Meim}_2]^+$ leads to a step by step bathochromic shift and a decreasing intensity of the CT band. A typical feature of **1b-**

$\text{Meim}_2]^+$ is the strong splitting of the band, presumably resulting from the low symmetry of the equatorial ligand (Figure 2).

EPR Measurements. The magnetic behavior and the EPR spectra at 77 K show the low-spin character ($S = 1/2$) of all the octahedral diadducts. The g values of the complexes $[\mathbf{1a-X}_2]^+$ ($g_1, 1.97-1.99$; $g_2, 2.05-2.14$; $g_3, 2.10-2.18$) are in the same range as those of the Schiff base complex **5** without electron-withdrawing substituents.

The crystal structure was determined for the complex $[\mathbf{1a-Him}_2]\text{PF}_6$.³² $[\mathbf{1a-Him}_2]\text{PF}_6$ has the axial imidazoles in perpendicular planes approximately over the $N_{\text{eq}}-\text{Fe}$ bonds. In the case of porphyrin derivatives, it is assumed that such an orientation leads to an equivalent interaction between the π donor orbitals of the axial ligand (e.g., imidazoles) and both d_{π} orbitals (d_{xz}, d_{yz}) of the ferric ion and determines the tetragonal symmetry of the complexes. Under this condition, the following EPR spectra are expected: for the electron configuration $(d_{xy})^2 (d_{xz}, d_{yz})^3$ a "strong g_{max} " spectrum with $g_{\text{max}} > 3.3$ ^{19,20} and for the configuration $(d_{xz}, d_{yz})^4 (d_{xy})^1$ an axial spectrum.^{21,22} In contrast to the predicted EPR spectra, the spectra of $[\mathbf{1a-Him}_2]\text{PF}_6$ are typically rhombic in methanol glass as well as in crystal. The adduct with ammonia (pure σ donor, without π donor/acceptor orbitals) shows this rhombic type of the spectra as well. Thus, the reason for the rhombic type is presumably not a special π interaction but rather the lower symmetry of the Schiff base ligand. The equatorial ligand in $[\mathbf{1a-X}_2]^+$ effects a strong tetragonal and rhombic distorted ligand field.

Walker et al.⁴³ studied the g values of low-spin porphyrin derivatives with different N heterocycles. In these cases, the EPR parameters depend on the ligand basicity and the special types of the heterocycle. The g values of bis(imidazole) and bis(aminopyridine) complexes show only small differences in dependence on the ligand basicity, while bis(pyrazole) and bis(indazole) complexes have g values that tend to converge if the basicity increases. In the case of the diadducts $[\mathbf{1a-X}_2]^+$, the ligand type determines the g values as well. However, within one type, e.g., with pyridine derivatives, the g values diverge with increasing basicity or decreasing π acceptor strength in the order $3\text{CNpy} < \text{na} < \text{py} < \text{dmap}$. Comparing the behavior of the diadducts of the π donor imidazole and the π acceptor phosphine, the spectra of the porphyrin derivatives and those of $[\mathbf{1a-X}_2]^+$ show the same trends. The g values diverge with decreasing π acceptor strength (see Table 1 and 2). These facts allow the following conclusions: (1) The EPR spectra of $[\mathbf{1a-X}_2]^+$ are mainly influenced by the π acceptor strength of the axial ligands. (2) In the case of porphyrin diadducts, the same trends in the g values were found when the axial ligands show large differences in their π acceptor strength. In the case of diadducts with similar types of axial ligands (e.g., imidazoles), the change in the g values is effected by the basicity of these ligands and shows the opposite trend. Because the porphyrin ligand itself is a weaker ligand than Schiff bases, a π interaction between the d_{π} orbitals of the central atom and the π acceptor orbitals of the axial ligands will be generally weak. Therefore, the basicity of axial ligands determines change in the g values, apart from strong π acceptors, such as phosphines, which leads to a convergence of the g values. In contrast to this, the equatorial Schiff base ligands are stronger donors. In this case, an interaction with the π acceptor orbitals of the axial ligands is significantly stronger, whereas the differences in the donor strength of the axial ligands are approximately leveled.

(42) For the spin-coupling constant, a value of 400 cm^{-1} was taken.^{16,26}

(43) Walker, F. A.; Reis, D.; Balke, V. L. *J. Am. Chem. Soc.* **1984**, *106*, 6888-6898.

In the same way, another phenomenon is explainable. In the case of the Schiff base complexes, the EPR spectra of the adducts with phosphorus ligands show superhyperfine splittings. The coupling constants amount to 18–24 [1a-(PR₃)₂]⁺ and 28–34 G [1a-(P(OEt)₃)₂]⁺, respectively. Neither in the case of synthetic porphyrins⁴⁴ nor in the case of natural derivatives⁴⁵ was such coupling proved. The observed coupling is presumably due to a strong covalency, effected by a π back-bonding between the axial acceptor ligand and the central atom. Understandably, the back-bonding is favored by strong donor ligands in the equatorial plain. As expected, the interaction is larger in the adducts with the stronger π acceptor phosphite than with phosphines.

With the step-by-step replacement of the ethylene bridges (X, Y) by phenylene bridges in the equatorial ligand, which leads to an increasing acceptor strength and a decreasing basicity of the macrocyclic anions, the complexes show a closer relationship to the porphyrins. The g values diverge in the order [1b-Meim₂]⁺ ($g = 1.960, 2.134, 2.212$) < [1c-Meim₂]⁺ ($g = 1.899, 2.136, 2.424$) < [FeTPP-Meim₂]⁺ ($g = 1.549, 2.294, 2.886$). The increasing electronegativity, as in the case of the [N₂O₂] donor set in the complex [7-Him₂]⁺ ($g = 1.94, 2.10, 2.40$), also leads to a divergence of the g values in comparison to [1a-Meim₂]⁺.

Relative Energies of the t_{2g} Orbitals. The relative energies of the t_{2g} orbitals were calculated from the g values using Taylor's hole model²³ (Table 3). The normalization condition ($a^2 + b^2 + c^2 = 1$) is fulfilled by taking the errors of g (Δg) in consideration.

The relative energies and the influence of the axial and the equatorial ligands on the splitting of the t_{2g} orbitals will now be discussed. Of course, the above-mentioned trends in the case of g values are reflected here.

The influence of the axial ligands on the splitting of the t_{2g} orbitals is not easy to explain, because different features of the ligand, such as basicity (σ donor strength), the π donor and π acceptor strength, and the ionic charge, must be considered. Thus, only similar axial ligands are compared here. The ammonia adduct is used as the standard (NH₃ is a pure σ donor, $E_1 = 4600, E_2 = 6800$ cm⁻¹). All anions, except for CN⁻, show a smaller splitting (E_2) independent of their basicity. The CN⁻ ion, which is defined usually as a strong π acceptor and shows a basicity similar to NH₃ ($pK_a = 9.25$), forms diadducts with a significantly greater E_2 (9600 cm⁻¹). In the case of pyridine derivatives, the observed increasing E_2 in the order dmap < py < na < 3CNpy could be explained with a decreasing basicity or with an increasing π acceptor strength of the pyridines. Ligands, such as isonitriles, phosphines, and phosphites, that are known as π acceptors effect strong increasing E_2 values ($E_2 = 16\ 000, 18\ 000, \text{ and } 28\ 000$ cm⁻¹).

With the step-by-step replacement of the ethylene bridges (R, R') by phenylene bridges in the equatorial ligand, the complexes show a closer relationship to the porphyrins. The orbital splitting decreases in the order [1a-X₂]⁺ > [2-X₂]⁺ > [3-X₂]⁺ > [FeTPP-X₂]⁺. This trend is in contrast to the effect of the axial ligands.

Correlation between the CT Energy and the t_{2g} Orbital Splitting. A discussion of the correlation between the CT energy and the t_{2g} orbital splitting follows.

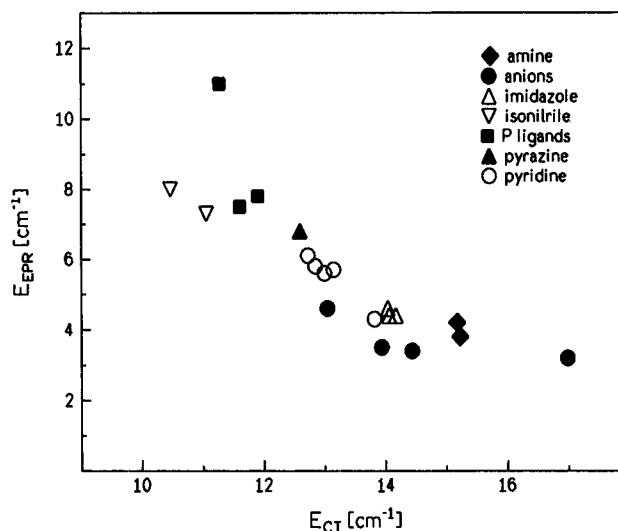
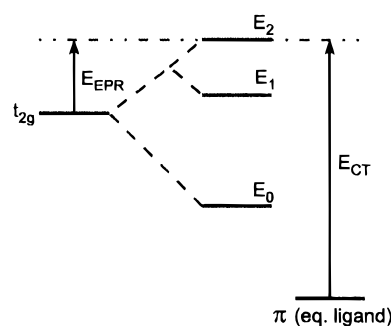


Figure 5. Energy E_{EPR} vs the CT energy.

Scheme 3



Schejter and Eaton²⁵ first tried to demonstrate such a correlation with some cytochrome *c* derivatives. Gadsby and Thomson²⁶ evaluated more extensive data. They investigated hemoproteins and their derivatives with one axial histidine and different second ligands (methionine, lysine, histidine, CN⁻, im⁻, OH⁻, N₃⁻, SH⁻, PhO⁻).

Gadsby and Thomson made the following assumptions: (1) The axial ligands do not influence the energy of the π orbitals of the equatorial ligand. (2) The d_{yz} is the hole orbital. (3) The CT energy E_{CT} corresponds to the transfer between the highest occupied π orbital of the equatorial ligand and the positive hole of the t_{2g} orbitals of the central atom. (4) The relative energies of the t_{2g} orbitals are calculated by means of Taylor's theory. The energy E_{EPR} is the energy of the hole orbital relative to the center of gravity of the t_{2g} orbitals. Scheme 3 shows the energy levels and defines the correlated energies. Accordingly, there should be a correlation between the energy E_{EPR} and the charge-transfer energy E_{CT} . Gadsby and Thomson found a linear relationship between both energies with a correlation coefficient of 0.89. Furthermore, they found that the CT energy is influenced more strongly by the investigated axial ligands than by the orbital splitting.

The wide range of diadducts [1a-X₂]⁺ made it possible to extend Thomson's correlation with very different axial ligands (for example, MeO⁻, CN⁻, NH₃, py, Him, PR₃, P(OEt)₃, and RNC). The energies E_{EPR} of these complexes are given in Table 4. In contrast to Thomson's assumptions, the character of the hole orbital is ambiguous (see above discussion). Figure 5 shows the plot of the energy E_{EPR} vs the CT energy. The represented correlation is totally different in comparison to the relationship of the hemoprotein derivatives. The energy E_{EPR} increases, when the CT energy decreases.

(44) Simonneaux, G.; Sodano, P. *Inorg. Chem.* **1988**, *27*, 3956–3959.

(45) Mansuy, D.; Duppel, W.; Ruf, H. H.; Ullrich, V. *Hoppe-Seyler's Z. Physiol. Chem.* **1974**, *355*, 1341–1349. Ruf, H. H.; Wende, P. *J. Am. Chem. Soc.* **1976**, *99*, 5499–5500. Sono, M.; Dawson, J. H.; Hager, L. *P. Inorg. Chem.* **1985**, *24*, 4339–4343.

(46) Walker, F. A.; Lo, M.-W.; Ree, M. T. *J. Am. Chem. Soc.* **1976**, *98*, 5552–5561.

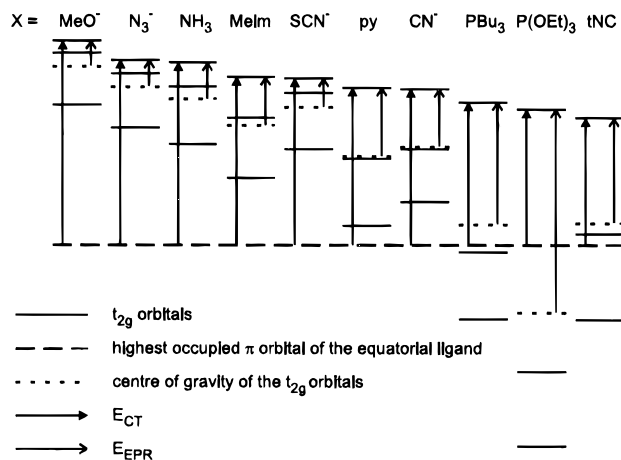


Figure 6. t_{2g} orbital splitting of $[1a-X_2]^+$.

To explain this, Figure 6 shows the orbital energies relative to the highest occupied ligand π orbital of the equatorial ligand. For simplification it was assumed that this orbital is not influenced by the axial ligands. The plot illustrates the following trends: (1) The center of the t_{2g} orbital energies increases as the basicity and π donor strength of the axial ligand increase and decreases as the π acceptor strength increases. (2) The maximal splitting (E_2) only increases with increasing π acceptor strength. It does not change significantly for different strong basic ligands without π acceptor properties. (3) The CT absorption shows a hypsochromic shift with increasing donor strength and a weaker bathochromic shift with increasing π acceptor strength of the axial ligand. The change in the CT energy is the opposite of that of the orbital splitting. (4) The π acceptor effect of the axial ligand influences the orbital splitting more than the opposite shift of the center of the orbital energies.

Finally, we will try to explain the differences between Thomson's correlation and that of the complexes $[1a-X_2]^+$.

The influence of the axial ligands on the CT absorption is probably the same in both cases. Axial donors increase the electron density at the central atom. The energy of the d orbitals and therefore the electron transfer energy from the equatorial ligand to the t_{2g} orbitals increase. The opposite effect is found in the case of acceptor ligands.

Orbital splitting in the case of the hemoprotein derivatives originates mainly from the π donor effect of the axial ligand. A stronger π donor leads to a stronger splitting and Gadsby and Thomson²⁶ found a linear relationship between the CT energy and the t_{2g} orbital splitting. However, this is only true for a limited number of axial ligands (histidine and another ligand). The relationship is not valid, however, for the adducts $[FeTPP-MeIm_2]^+$ and $[FeTPP-(PMe_3)_2]^+$ with a large difference of the π donor/acceptor strength of the axial ligands. In this case, the increasing orbital splitting is dominated by the increasing π acceptor strength. This behavior is also found in the derivatives of $[1a-X_2]^+$ with axial ligands that show smaller differences of the π donor/acceptor strength. The splitting of the t_{2g} orbitals is first influenced by the equatorial ligand. This is due to the strong basic character and the low symmetry of the equatorial ligand. The high basicity leads to a higher electron density of the t_{2g} orbitals. Thus, the axial π acceptors increase the orbital splitting, whereas the axial π donors have only a small influence on it. Therefore, as the CT energy increases, the orbital splitting decreases.

Acknowledgment. This work was supported by the Deutsche Forschungsgemeinschaft and the Fonds der Chemischen Industrie. H.K. acknowledges a grant from the Fonds der Chemischen Industrie.

IC9702633